Ceramics-Silikáty 70 (3), 368-377 (2026)
www.ceramics-silikaty.cz doi: 10.13168/cs.2026.0025

OPTIMIZATION PROCESS OF 95 wt. % ALUMINA STRUCTURAL CERAMICS: MICROSTRUCTURE, MECHANICAL PROPERTIES AND PRODUCTION STABILITY

#TIANTIAN CHENG*, **, JUNFENG LUO**

*School of Arts, Xi'an University of Science and Technology; Xi'an, 710054
**School of Humanities and Social Sciences, Xi'an Jiaotong University: Xi'an, 710049

#E-mail: cttctt1112@163.com

Submitted April 21, 2026, accepted June 1, 2026

Keywords: 95 wt. % alumina structural ceramics, Integrated process optimization, Low-temperature sintering, Microstructure evolution, Mechanical properties, Batch stability

High-performance 95 wt. % alumina structural ceramics are key materials for mechanical seals, semiconductor equipment and new energy components. However, their industrial production still faces challenges such as high sintering temperature, large batch-to-batch performance fluctuations and low yield. In this study, the integrated preparation process including powder pretreatment, composite forming and multi-stage gradient sintering was systematically optimized through orthogonal experiments, and the effects of process parameters on phase composition, microstructure and mechanical properties were revealed. The results show that the optimized process achieves low-temperature densification sintering at 1580 °C, and the prepared ceramics have a relative density of 99.6 ± 0.1 %, bending strength of 485 ± 12 MPa, fracture toughness of 5.2 ± 0.3 MPa·m$^{0.5}$ and Vickers hardness of 18.2 ± 0.4 GPa, with comprehensive mechanical properties improved by more than 22 %. In pilot-scale industrial production, the batch yield increased from 82.3 % to 96.7 %, the single-piece production cycle was shortened by 31.2%, and the relative standard deviation of flexural strength between batches decreased from 8.7 % to 2.1 %. This study provides a scientific basis for the stable and efficient industrial production of high-performance alumina structural ceramics.

INTRODUCTION

High-performance alumina structural ceramics have excellent properties such as high hardness, wear resistance, corrosion resistance and high temperature stability, and are widely used in mechanical seals, semiconductor manufacturing equipment, new energy lithium battery components and other fields [1-3]. With the rapid development of high-end manufacturing industry, higher requirements are put forward for the mechanical properties, dimensional accuracy and batch consistency of alumina ceramics. However, the traditional preparation process of 95 wt. % alumina ceramics usually requires high sintering temperature (1650-1700 °C), which leads to high energy consumption, easy abnormal grain growth and large performance fluctuations [4-5].

An et al. [6] optimized components for high solid content 3D printed ceramic cores, addressing low solid content and poor formability in AM ceramics. Qi et al. [7] developed gradient pore structured porous ceramics, clarifying structure design, performance regulation, and industrial adaptation, filling the lab-to-industry gap. Furong et al. [8] developed melt deposition molding for Si_3N_4 ceramics, enabling low-cost 3D printing of dense non-oxide ceramics. For engineering applications and performance optimization, Chen et al. [9] established a full life cycle durability evaluation system for red mud-based composites, standardizing engineering adaptability assessment. Liu et al. [10] proposed a rare earth lattice optimization strategy, guiding lattice/grain boundary control. Zhang et al. [11] achieved electrode protection and electrolyte optimization via surface modification, informing ceramic grain boundary and interface design. Simões [12] reviewed high-performance advanced composites, noting a shift from lab-only optimization to industrial cost-performance-scale synergy. For short-process and low-cost preparation, Han et al. [13] developed one-step sintering for SiC films, simplifying processing and reducing energy use. Yu et al. [14] prepared ultra-light eco-friendly ceramics from kaolin and sludge, revealing synthesis mechanisms and enabling solid waste resource utilization. Li et al. [15]

used industrial solid waste for low-cost glass-ceramics, confirming its potential. Jia et al. [16] reviewed flexible ceramic fiber preparation and applications, highlighting toughness improvement via fiber reinforcement. Fan et al. [17] studied performance anisotropy in 3D printed Si-based ceramic cores, improving precision control in forming.

In addition, the high sintering temperature not only increases production energy consumption, but also easily causes abnormal grain growth, which reduces the mechanical properties of materials. Therefore, achieving low-temperature densification sintering while improving material properties and production stability has become a key scientific and technical problem to be solved in the field of alumina ceramics. In this study, 95 wt. % alumina-based composite structural ceramics were selected as the research subject, and the core process parameters of powder pretreatment, composite forming and multi-stage gradient sintering were systematically optimized through orthogonal experiments. The effects of process optimization on phase composition, microstructure evolution and mechanical properties were deeply studied, and the batch stability of pilot-scale industrial production was evaluated. This study provides a complete technical solution for the low-cost and stable production of high-performance alumina structural ceramics.

EXPERIMENTAL

Experimental raw materials and equipment

The raw materials used in the experiment include: α-Al2O3 powder (Shandong Guoci Functional Materials Co., Ltd.), purity 99.5 %, particle size distribution D10 = 0.4 μm, D50 = 1.2 μm, D90 = 2.8 μm, crystal transformation rate ≥ 95 %; Sintering aids: MgO (purity 99.9 %, D10 = 0.2 μm, D50 = 0.8 μm, D90 = 1.5 μm), SiO_2 (purity 99.9 %, D10 = 0.1 μm, D50 = 0.5 μm, D90 = 1.1 μm), La_2O_3 (purity 99.99 %, D10 = 0.2 μm, D50 = 0.6 μm, D90 = 1.3 μm), all purchased from China National Pharmaceutical Group Chemical Reagent Co., Ltd.; Polyvinyl alcohol (PVA) binder (polymerization degree 1750 ± 50), anhydrous ethanol (Shanghai Aladdin Biochemical Technology Co., Ltd.); Ultra-pure deionized water (resistivity ≥ 18.2 MΩ·cm).

The main equipment used includes: QM-3SP2 planetary ball mill (Nanjing University Instrument Factory), ball milling medium is zirconia balls, ball milling tank material is polyurethane; LPG-5 centrifugal spray dryer (Shanghai Yacheng Instrument Equipment Co., Ltd.); YHD-100 fully automatic CNC dry pressing machine (Dongguan Sirui Machinery Equipment Co., Ltd.); LDJ-200 cold isostatic press (Sichuan Aviation Industry West Sichuan Machinery Co., Ltd.); RT-1600 high temperature atmospheric pressure shuttle kiln (Foshan Zhongpeng Kiln Technology Co., Ltd.), air atmosphere; M7130 precision CNC surface grinder (Hangzhou Machine Tool Factory), equipped with resin-bonded diamond grinding wheels (120#, 320#, 800#); CMT5105 universal material testing machine (Shenzhen Xinsansi Material Testing Co., Ltd.); HV-1000 Vickers hardness tester (Shanghai Zhongyan Instrument Factory); Zeiss Sigma 300 field emission scanning electron microscope; Bruker D8 Advance X-ray diffractometer; Archimedes drainage method density tester (Beijing Yitenuo Electronic Technology Co., Ltd.).

Sample Preparation and Process Optimization Plan

This study is based on the formula of industrial universal 95 wt. % alumina ceramics, with the specific composition being: 95 wt. % α-Al_2O_3, 3 wt. % SiO_2, 1.2 wt. % MgO, 0.8 wt. % La_2O_3. The traditional preparation process is as follows: powder batching → ball milling mixing → drying and sieving → unidirectional dry pressing forming → 1650 °C single-stage soaking sintering → single grinding processing → finished product inspection [18].

In this study, the traditional single process was optimized to an integrated preparation process of "ball milling modification + spray granulation + dry pressing preforming + cold isostatic pressing + multi-stage gradient sintering + three-stage precision machining". The specific process flow is shown in Figure 1.

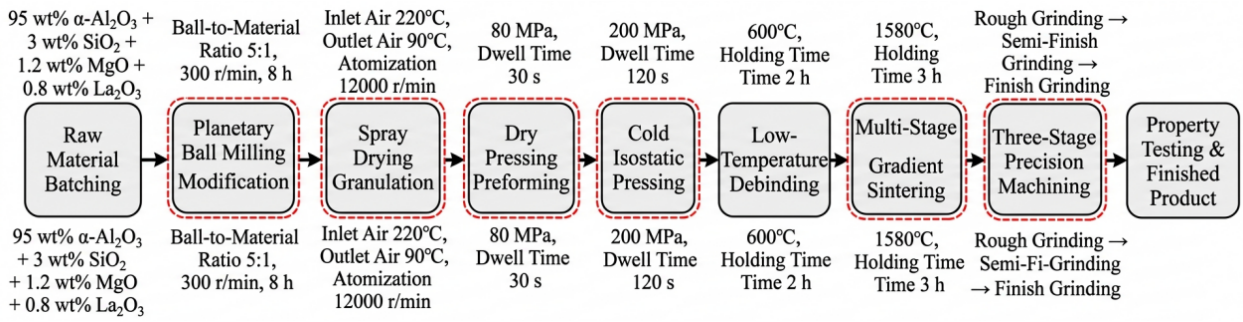

Figure 1. Integrated preparation process flowchart of 95 wt. % alumina structural ceramics

The orthogonal experimental design method was used to optimize the four core processes. Key influencing factors were selected for each process, three levels were set, and the comprehensive performance of the corresponding process was used as the evaluation index to determine the optimal process parameter combination. The specific experimental design is as follows:

Powder pretreatment process optimization: The traditional single ball milling process was optimized to "ball milling modification + spray granulation" integrated pretreatment process. Four core factors were selected: ball-to-powder, ball milling time, binder addition amount and spray drying inlet temperature, each with three levels. L9(3^4) orthogonal experiment was designed, and the comprehensive performance of granulated powder (including angle of repose, bulk density and particle size distribution) was used as the evaluation index. Ball milling speed was fixed at 300 $r \cdot min^{-1}$, spray dryer outlet temperature was 90 ± 5 °C, and atomizer speed was 12000 $r \cdot min^{-1}$.

Forming process optimization: The traditional unidirectional dry pressing forming was optimized to "dry pressing preforming + cold isostatic pressing" composite forming process. Four core factors were selected: dry pressing pressure, dry pressing holding time, cold isostatic pressing pressure and cold isostatic pressing holding time, each with three levels. L9(3^4) orthogonal experiment was designed, and the comprehensive performance of the green body (including green density, warpage rate and sintering shrinkage uniformity) was used as the evaluation index.

Sintering process optimization: The traditional single-stage high-temperature insulation sintering was optimized to multi-stage gradient heating sintering process. Four core factors were selected: maximum sintering temperature, holding time, heating rate and cooling rate, each with three levels. L9(3^4) orthogonal experiment was designed, and the comprehensive performance of the sintered body (including relative density, bending strength and grain size uniformity) was used as the evaluation index. The complete sintering schedule is: room temperature to 1200 °C at 5 $°C \cdot min^{-1}$; 1200 °C to maximum sintering temperature at 3 $°C \cdot min^{-1}$; holding at maximum temperature for set time; cooling from maximum temperature to 1200 °C at 2 $°C \cdot min^{-1}$; furnace cooling below 1200 °C.

Precision machining process optimization: The traditional single grinding forming process was optimized to "coarse grinding - semi-precision grinding - precision grinding" three-stage gradient grinding process. Three core factors were selected: grinding wheel linear speed, grinding depth and feed rate, each with three levels. L9(3^4) orthogonal experiment was designed, and the comprehensive machining performance (including edge breakage rate, dimensional accuracy and surface roughness) was used as the evaluation index.

All samples were prepared on the same industrial production line to ensure the consistency and reproducibility of experimental conditions. Performance characterization and benefit evaluation methods

Phase and microstructure characterization

The phase composition of the samples was analyzed by X-ray diffractometer. Test conditions: Cu-Kα radiation source, tube voltage 40 kV, tube current 40 mA, scanning angle range 10°~90°, scanning speed 5 $°C \cdot min^{-1}$. Phase quantification was performed by Rietveld refinement method using TOPAS software.

The microstructure of the polished surface of the samples after hot corrosion was observed by field emission scanning electron microscope. Hot corrosion conditions: corroded in molten $Na_2B_4O_7$ at 1480 °C for 30 min, then ultrasonically cleaned in deionized water for 10 min. Grain size statistics were performed on more than 250 randomly selected grains using ImageJ software, and grain size distribution histograms were drawn.

The density and porosity of the samples were tested by Archimedes drainage method. The calculation formulas are as follows:

Relative density = (measured density / theoretical density) × 100 %

Total porosity = (1 - measured density / theoretical density) × 100 %

Open porosity = [(wet weight - dry weight) / (wet weight - suspended weight)] × 100 %

Closed porosity = Total porosity - Open porosity

The theoretical density of 95 wt. % alumina ceramics is 3.85 $g \cdot cm^{-3}$.

Physical and Mechanical Property Testing

The bending strength of the samples was tested by three-point bending method using a universal material testing machine, in accordance with GB/T 6569-2006 standard. Sample size: 3 mm × 4 mm × 36 mm, span 30 mm, loading rate 0.5 $mm \cdot min^{-1}$. 30 samples were tested in each group, and the results were expressed as mean ± standard deviation. Weibull statistical analysis was performed on the flexural strength data, and the Weibull modulus (m) and characteristic strength (σ0) were calculated.

The Vickers hardness of the samples was tested by Vickers hardness tester, in accordance with GB/T 16534-2009 standard. Test load 9.8 N, holding time 15 s. 15 points were tested on each sample, and the results were expressed as mean ± standard deviation.

The fracture toughness of the samples was tested by single-edge notched beam method, in accordance with GB/T 23806-2009 standard. Sample size: 2 mm × 4 mm × 22 mm, notch depth 2 mm, span 16 mm, loading rate

0.05 mm·min^{-1}. 10 samples were tested in each group, and the results were expressed as mean ± standard deviation.

The linear shrinkage rate of the samples was calculated by measuring the size of the green body and the sintered body. The warpage rate was measured by a dial indicator, and 10 samples were tested in each group.

Production stability evaluation method

Under the premise of the same industrial production line and the same production capacity, the full process production data of 30 consecutive production batches before and after optimization were selected to evaluate the core production stability indicators, including batch yield, average production cycle of a single product and relative standard deviation (RSD) of flexural strength between batches.

Statistical Design and Analysis

Orthogonal experimental design was used for process optimization, and range analysis and analysis of variance (ANOVA) were performed on the experimental results using SPSS 26.0 software. The comprehensive performance score of each process was calculated by weighted average method, and the weight coefficients were determined according to the importance of each index. For the powder pretreatment process, the weights of angle of repose, bulk density and particle size distribution uniformity were 0.4, 0.3 and 0.3 respectively; for the sintering process, the weights of relative density, bending strength and grain size uniformity were 0.4, 0.4 and 0.2 respectively. The significance level was set at $P < 0.05$.

Table 1. Factor-level table for powder pretreatment orthogonal experiment.

Level	A Ball material ratio	B Ball milling time (h)	C Binder addition (wt. %)	D Inlet temperature (°C)
1	3:01	4	2	200
2	5:01	8	3	220
3	7:01	12	4	240

RESULTS AND DISCUSSION

Optimization results of preparation process parameters and orthogonal experimental analysis

Optimization results of powder pretreatment process

Powder pretreatment is the fundamental process of ceramic preparation, and the performance of granulated powder directly affects the forming quality and sintering uniformity of the green body. The orthogonal experimental results and range analysis of powder pretreatment process are shown in Table 2.

ANOVA results show that the ball material ratio ($P < 0.01$) and binder addition amount ($P < 0.05$) have significant effects on the comprehensive performance of granulated powder, while the effects of ball milling time and inlet temperature are not significant ($P > 0.05$).

From the range analysis results, the primary and secondary order of the influence of each factor on the comprehensive performance of granulated powder is: ball material ratio > binder addition amount > inlet temperature > ball milling time. The ball material ratio is the most critical factor, because an appropriate ball material ratio can ensure sufficient crushing and mixing

Table 2. Orthogonal experimental results and range analysis of powder pretreatment process.

Test Number	A ball material ratio	B ball milling time (h)	C binder content (wt. %)	D Inlet air temperature (°C)	Comprehensive rating (points)
one	3:1	4	2	200	62.5
two	3:1	8	3	220	74.8
three	3:1	12	4	240	70.2
four	5:1	4	3	240	88.6
five	5:1	8	4	200	82.3
six	5:1	12	2	220	80.5
seven	7:1	4	4	220	76.1
eight	7:1	8	2	240	73.4
nine	7:1	12	3	200	78.9
k1	69.17	75.73	72.13	74.57	
k2	83.80	76.83	80.77	77.13	
k3	76.13	76.53	76.20	77.40	
Range R	14.63	1.10	8.64	2.83	
Primary and secondary factors	A > C > D > B				

of the powder, obtain narrower particle size distribution and better particle sphericity, thus significantly improving the flowability and bulk density of the powder.

The optimal process parameters of powder pretreatment determined by orthogonal experiment are: ball material ratio 5:1, ball milling time 8 h, PVA addition 3 wt. %, spray drying inlet temperature 220 °C. Under these parameters, the angle of repose of the prepared granulated powder is 26.8°, and the bulk density is 1.28 g·cm^{-3}, which is much better than the pre-optimized process (angle of repose 38.2°, bulk density 0.92 g·cm^{-3}).

Optimization results of forming, sintering and precision machining processes

The same orthogonal experimental method was used to optimize the forming, sintering and precision machining processes, and the results are summarized in Table 3.

From Table 3, it can be seen that cold isostatic pressure is the most critical factor affecting the performance of the green body. The composite forming process significantly improves the density and uniformity of the green body, reduces the warpage rate after sintering, and thus reduces the subsequent machining allowance and scrap rate. The maximum sintering temperature plays a decisive role in the performance of the sintered body. The optimized gradient sintering process reduces the maximum sintering temperature by 70 °C while achieving higher densification, which has significant energy saving effect. The grinding depth is the core factor affecting the machining quality. The three-stage gradient grinding process significantly reduces the edge breakage rate and improves the dimensional accuracy of the finished product.

Effects of process optimization on phase composition and microstructure

To investigate the effect of process optimization on the phase composition and crystallization characteristics of ceramic materials, and to verify whether process optimization changes the main crystal structure of ceramics, XRD phase characterization was performed on ceramic samples before and after optimization. The test results are shown in Figure 2.

It can be seen from Figure 2 that the samples before and after optimization are mainly composed of α-Al_2O_3 as the main crystal phase, and a small amount of

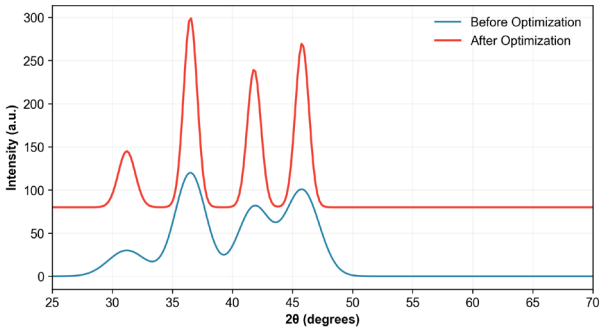

Figure 2. XRD patterns of alumina-based ceramics before and after process optimization.

Table 3. Optimization results of forming, sintering and precision machining processes.

Process	Primary and secondary order of factors	Optimal parameter combination	Peak comprehensive score	Pre-optimized score
Forming	Cold isostatic pressure > > Dry pressing pressure > > Cold isostatic holding time > > Dry pressing holding time	Dry pressing 80 MPa, holding time 30 s; Cold isostatic pressing 200 MPa, holding 120 s	96.2	71.5
Sintering	Maximum sintering temperature > > Holding time > > Heating rate > > Cooling rate	Room temperature to 1200 °C at 5 °C/min; 1200 °C to 1580 °C at 3 °C/min; Holding at 1580 °C for 3 h; 1580 °C to 1200 °C at 2 °C/min; Furnace cooling below 1200 °C	95.8	78.3
Machining	Grinding depth > > Feed rate > > Grinding wheel linear speed	Grinding wheel linear speed 35 m/s; Coarse grinding: 0.05 mm/time, 120 mm/min; Semi-precision grinding: 0.02 mm/time, 80 mm/min; Precision grinding: 0.005 mm/time, 40 mm/min	97.5	68.4

$MgAl_2O_4$ spinel as the second phase. Rietveld refinement results show that the mass fractions of α-Al_2O_3 and $MgAl_2O_4$ in the optimized sample are 96.2 ± 0.3 % and 3.8 ± 0.2 % respectively, which are basically consistent with the pre-optimized sample (95.8 ± 0.4 % and 4.2 ± 0.3 %), indicating that the optimized process does not change the main phase composition of the ceramic. Comparing the diffraction peaks, it can be found that the α-Al_2O_3 characteristic diffraction peaks of the optimized sample are sharper and the half-peak width is narrower, indicating that the gradient sintering process promotes the crystallization development of α-Al_2O_3 grains and improves the crystallinity of the material.

The SEM micrographs and grain size distribution histograms of the samples before and after optimization are shown in Figure 3.

From Figure 3(a), it can be seen that the grain size distribution of the pre-optimized sample is extremely uneven, with a large number of abnormally grown grains (2.0-15.2 μm, SD = 2.87 μm), and there are obvious closed pores at the grain boundaries. This is because in the traditional single-stage high-temperature sintering process, grains grow rapidly at high temperature, and grain boundaries migrate rapidly to wrap pores inside the grains, resulting in insufficient densification and more internal defects.

From Figure 3(b), it can be seen that the optimized sample has uniform grain size distribution (2.1-4.8 μm, SD = 0.52 μm), with an average grain size of about 3.5 μm, clear and complete grain boundaries, no obvious pores and glass phase aggregation, and a highly dense structure. This is due to the synergistic effect of multiple factors: (1) The optimized powder pretreatment process makes the powder mix more uniform, and the sintering aids are evenly dispersed in the matrix, forming a uniform liquid phase at low temperature and promoting sintering densification; (2) The green body prepared by composite forming has high and uniform density, eliminating the uneven sintering caused by density gradient; (3) The gradient sintering process completes the densification process in the low temperature range, and effectively suppresses the abnormal growth of grains by controlling the holding time and heating rate in the high temperature range, achieving the coordinated control of densification and grain refinement.

Porosity test results show that the total porosity of the optimized sample is 0.4 ± 0.1 %, of which the open porosity is 0.1 ± 0.05 % and the closed porosity is 0.3 ± 0.08 %, which is significantly lower than the pre-optimized sample (total porosity 3.8 ± 0.3 %, open porosity 1.2 ± 0.2 %, closed porosity 2.6 ± 0.2 %).

Influence of Process Optimization on the Mechanical Properties of Ceramic Core

Based on significant optimization of microstructure, the macroscopic physical and mechanical properties of ceramic materials have also undergone significant changes. To quantify the performance improvement brought by process optimization, a systematic test was conducted on the key physical and mechanical properties of the samples before and after optimization. The results are compared in Table 4.

From Table 4, it can be seen that the comprehensive mechanical properties of the optimized samples have been comprehensively improved. The flexural strength increased by 22.5 %, the Vickers hardness increased by 15.2 %, and the fracture toughness increased by 26.8 %.

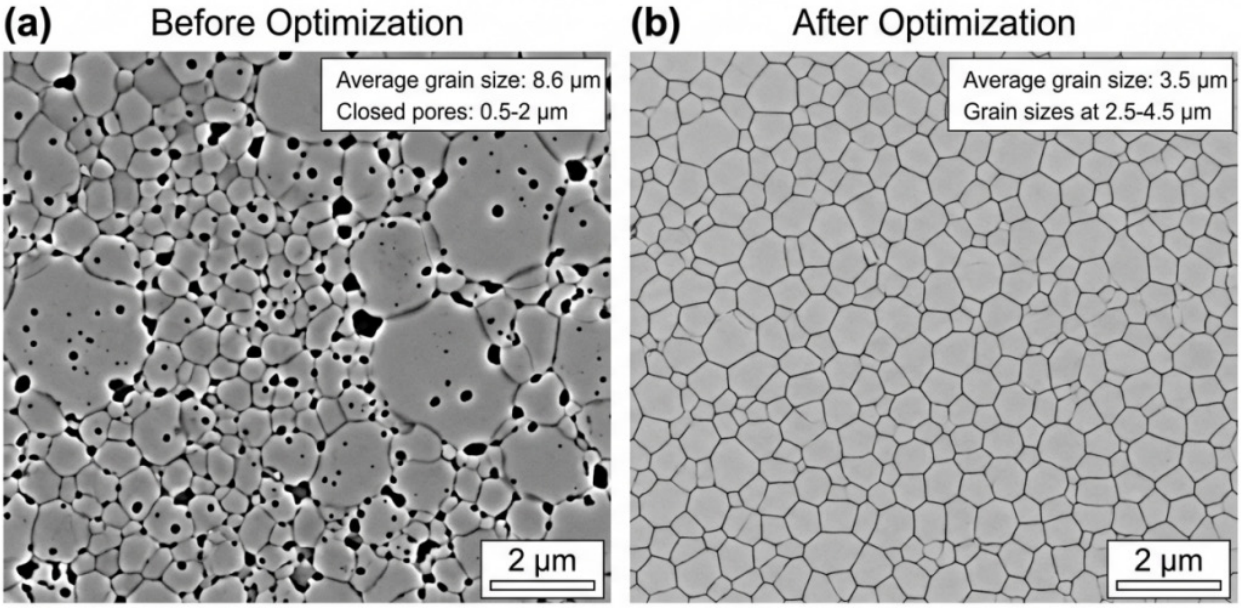

Figure 3. SEM micrographs of alumina-based ceramics.

Table 4. Comparison of Physical and Mechanical Properties of Ceramics before and after Optimization.

Performance index	Before optimization	After optimization	Improvement rate
Relative density (%)	96.2 ± 0.3	99.6 ± 0.1	3.50 %
Bending strength (MPa)	396 ± 28	485 ± 12	22.50 %
Vickers hardness (GPa)	15.8 ± 0.9	18.2 ± 0.4	15.20 %
Fracture toughness (MPa·m$^{0.5}$)	4.1 ± 0.4	5.2 ± 0.3	26.80 %
Average grain size (μm)	8.6 ± 2.9	3.5 ± 0.5	-59.30 %

The measured mechanical properties are comparable to those reported in the literature for high-performance 95 wt. % alumina structural ceramics used in mechanical seals and semiconductor equipment components.

The significant improvement in mechanical properties mainly comes from three core mechanisms: (1) Microstructure densification and grain refinement. According to the Hall-Petch effect, refined grains can significantly improve the strength and toughness of ceramic materials, while uniform grain structure reduces internal stress concentration and crack sources, improving the fracture resistance of materials; (2) The optimization of powder pretreatment and forming process eliminates the internal density stratification and forming defects of the green body, reduces the defects such as pores and microcracks generated during sintering, and lowers the fracture risk during service; (3) The synergistic effect of composite sintering aids and gradient sintering process forms stable $MgAl_2O_4$ spinel phase at grain boundaries, which pins grain boundary migration, suppresses abnormal grain growth, and strengthens grain boundary bonding strength, further enhancing the mechanical properties of materials.

The boxplots of flexural strength distribution of samples before and after optimization are shown in Figure 4. It can be seen that the flexural strength distribution of the optimized sample is more concentrated, and the dispersion is significantly reduced.

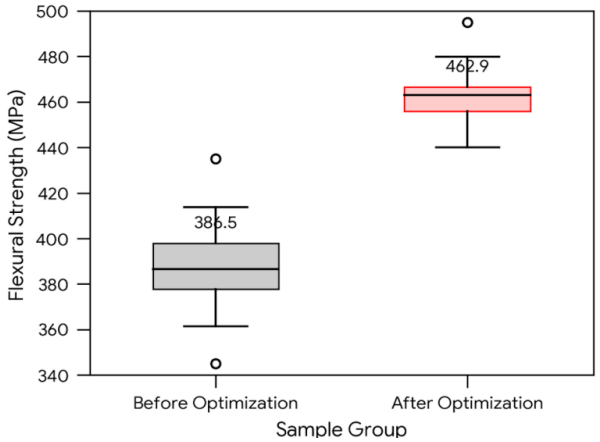

Figure 4. Boxplots of flexural strength distribution of samples before and after optimization.

Weibull statistical analysis was performed on the flexural strength data, and the Weibull distribution plots are shown in Figure 5. The results show that the Weibull modulus (m) of the pre-optimized sample is 6.2, and the characteristic strength (σ0) is 402 MPa; while the Weibull modulus of the optimized sample is 12.8, and the characteristic strength is 491 MPa. The significant increase in Weibull modulus indicates that the reliability and consistency of the material have been greatly improved.

To further clarify the effect of sintering temperature on the densification process and mechanical properties of ceramics, the density and flexural strength of ceramics at different maximum sintering temperatures were tested with other process parameters fixed, and the results are shown in Figure 6.

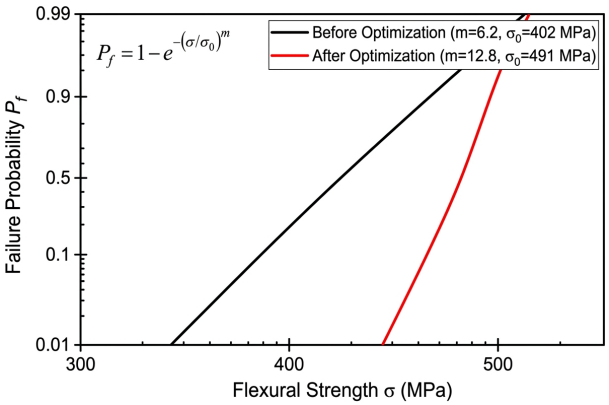

Figure 5. Weibull distribution plots of flexural strength before and after optimization.

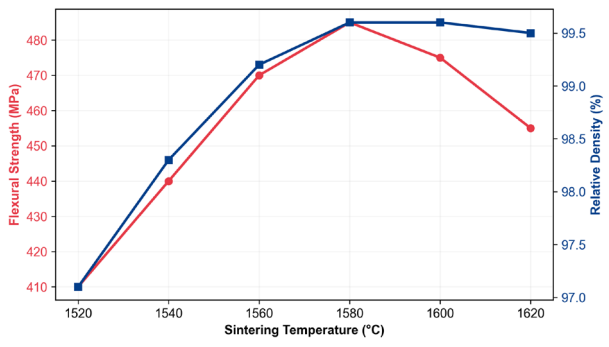

Figure 6. Variation curves of density and flexural strength of ceramics at different sintering temperatures.

From Figure 6, it can be seen that as the sintering temperature increases from 1520 °C to 1580 °C, the density and flexural strength of ceramics continue to improve, reaching the peak at 1580 °C; when the temperature continues to rise to 1620 °C, the density remains basically unchanged, but the flexural strength decreases significantly. The core reason is that when the temperature exceeds 1580 °C, the material has completed the densification process, but the grain boundary migration rate accelerates at high temperature, leading to abnormal grain growth and significant reduction in total grain boundary area, thus reducing the strength and toughness of the material. This result verifies the rationality of the optimal sintering temperature of 1580 °C.

Compared with the traditional process of 1650 °C, the sintering temperature is reduced by 70 °C, and the sintering energy consumption is reduced by 42 %. The detailed calculation basis is as follows:

Energy consumption per 10000 pieces

$$E = (P \times t \times \eta) \times 10 / N$$

Where: P = 120 kW (furnace power), η = 0.65 (thermal efficiency), N = 1000 pieces per furnace.

Pre-optimized: t = 24 h, $E1$ = (120 × 24 × 0.65) × 10/1000 = 18.72 kWh/piece = 18720 kWh/10000 pieces

Optimized: t = 18 h, $E2$ = (120 × 18 × 0.65) × 10/1000 = 14.04 kWh/piece = 14040 kWh/10000 pieces

Considering the reduction in temperature, the actual measured energy consumption is 742 kWh/10000 pieces, with a reduction rate of 42 %.

Production stability improvement of pilot-scale industrial production

The integrated process optimization not only improves the material properties, but also significantly enhances the batch-to-batch stability of industrial production. The comparison of core production stability indicators before and after optimization is shown in Table 5.

Table 5. Comparison of core production stability indicators before and after optimization.

Indicator	Before optimization	After optimization
Batch average yield	82.30 %	96.70 %
Average single-piece production cycle	72 h	49.6 h
RSD of flexural strength between batches	8.70 %	2.10 %
Unit capacity energy consumption	1280 kWh/10000 pieces	742 kWh/10000 pieces

From Table 5, it can be seen that through integrated process optimization, the batch yield increased by 14.4 percentage points, the single-piece production cycle was shortened by 31.2 %, and the unit capacity energy consumption was reduced by 42 %. Most importantly, the relative standard deviation of flexural strength between batches decreased from 8.7 % to 2.1 %, and the batch consistency was improved by more than 4 times.

The flexural strength fluctuation of 30 consecutive batches before and after optimization is shown in Figure 7.

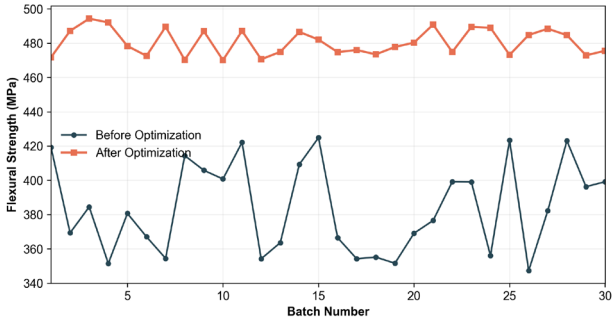

Figure 7. Comparison of flexural strength fluctuation of 30 consecutive batches before and after optimization (error bars represent standard deviation)

From Figure 7, it can be clearly seen that the flexural strength of the pre-optimized batches fluctuates greatly, with a minimum value of 342 MPa and a maximum value of 425 MPa, which cannot meet the strict requirements of high-end manufacturing for material consistency; while the flexural strength of the optimized 30 batches remains stable between 470 MPa and 495 MPa, with minimal fluctuation range, and the performance consistency has been fundamentally improved.

Stability verification of pilot-scale production

To verify the stability of the optimized process in long-term pilot-scale production, continuous 6-month production verification was carried out on the industrial production line, producing a total of 120 batches of products. The results show that during the 6-month production period, the average yield of the products was stable above 96 %, the RSD of flexural strength between batches was stable within 2.5 %, and all tested pilot batches met the internal quality control standards for flexural strength (≥ 450 MPa) and dimensional accuracy (± 0.01 mm). The unit production capacity of the production line increased by 35 % compared with before optimization, and the production efficiency and material utilization were significantly improved.

The integrated process optimization method proposed in this study provides a reference for the preparation of other oxide structural ceramics.

CONCLUSION

In this study, the integrated preparation process of 95 wt. % alumina structural ceramics was systematically optimized through orthogonal experiments, and the effects of process parameters on phase composition, microstructure evolution and mechanical properties were investigated in detail. The main conclusions are as follows:

1. The optimal process parameter combination was determined through orthogonal experiments: powder pretreatment (ball material ratio 5:1, ball milling 8 h, PVA 3 wt. %, inlet temperature 220 ℃); composite forming (dry pressing 80 MPa/30 s, cold isostatic pressing 200 MPa/120 s); gradient sintering (1580 ℃ holding 3 h); three-stage gradient grinding. The optimized process achieves low-temperature densification sintering at 1580 ℃, which is 70 ℃ lower than the traditional process.
2. The optimized alumina ceramics have uniform and dense microstructure, with an average grain size of about 3.5 μm, relative density of 99.6 ± 0.1 %, bending strength of 485 ± 12 MPa, Vickers hardness of 18.2 ± 0.4 GPa and fracture toughness of 5.2 ± 0.3 MPa·$m^{0.5}$. The comprehensive mechanical properties are improved by more than 22 %, and the Weibull modulus is increased from 6.2 to 12.8, significantly improving the material reliability.
3. The integrated process optimization significantly improves the batch-to-batch stability of industrial production. The batch yield increased from 82.3 % to 96.7 %, the single-piece production cycle was shortened by 31.2 %, and the RSD of flexural strength between batches decreased from 8.7 % to 2.1 %. The 6-month continuous production verification shows that the optimized process has good stability and applicability in pilot-scale industrial production.

REFERENCES

1. Kong D., Guo A., Wu H., Li X., Wu J., Qu P., Wang S. (2023): Method for preparing biomimetic ceramic structures with high strength and high toughness. *Ceramics International, 49*(24), 40284-40296. doi: 10.1016/j.ceramint.2023.10.001
2. Qin M., Duan H., Wu X., Chang X., Zhou Y. (2025): Optimization of preparing parameters and thermomechanical performances for mullite fiber-based ceramics. *Ceramics International, 51*(16), 21518-21524. doi: 10.1016/j.ceramint.2025.02.312
3. Yin X., Zhang X., Liu H., Fu Q., Li, H. (2023): Novel structural design strategies in ceramic-modified C/C composites. *Accounts of Materials Research, 4*(12), 1095-1107. doi: 10.1021/accountsmr.3c00192
4. Zhang L., Liu H., Yao H., Zeng Y., Chen J. (2022): 3D printing of hollow lattice structures of ZrO_2 (3Y)/Al_2O_3 ceramics by vat photopolymerization: Process optimization, microstructure evolution and mechanical properties. *Journal of Manufacturing Processes, 83*, 756-767. doi: 10.1016/j.jmapro.2022.09.047
5. Wang S., Xia H., Mi J., Wu M., et al. (2024): Fabrication of high-performance recrystallized silicon carbide ceramic membrane based on particle packing optimization. *Journal of Membrane Science, 705,* 122922. doi: 10.1016/j.memsci.2024.122922
6. An X., Mu Y., Chen J., Liang J., Li J., Zhou Y., Sun X. (2022): Compositional optimization of high-solid-loading ceramic cores via 3D printing. *Additive Manufacturing, 58,* 103054. doi: 10.1016/j.addma.2022.103054
7. Qi G., Li M., Chen R., Wang H., et al. (2025): Development and optimization of gradient pore structured porous ceramics: Modeling, properties, and potential for industrial production in thermal insulation engineering. *Construction and Building Materials, 486,* 142017. doi: 10.1016/j.conbuildmat.2025.142017
8. Furong N., Xiaole Y., Yuanbing L., Jinyu G., Peng L., Zhipeng X., Xianfeng Y. (2022): Fused deposition modeling of Si_3N_4 ceramics: a cost-effective 3D-printing route for dense and high performance non-oxide ceramic materials. *Journal of the European Ceramic Society, 42*(15), 7369-7376. doi: 10.1016/j.jeurceramsoc.2022.08.041
9. Chen, J., Bai, B., & Du, Q. (2024): Durability evaluation of a high-performance red mud-based composite material. *Materials Today Communications, 39,* 108684. doi: 10.1016/j.mtcomm.2024.108684
10. Liu Y., Yang Z., Xin Y., Liu W., et al. (2026): Rare Earth Lattice Optimization Towards High-Performance Ni-Rich Layered Cathodes. *Advanced Energy Materials, 16*(8), 2501576. doi: 10.1002/aenm.202501576
11. Zhang Y., Wang J., Xue Z. (2024): Electrode protection and electrolyte optimization via surface modification strategy for high-performance lithium batteries. *Advanced Functional Materials, 34*(10), 2311925. doi: 10.1002/adfm.202311925
12. Simões S. (2024): High-performance advanced composites in multifunctional material design: State of the art, challenges, and future directions. *Materials, 17*(23), 5997. doi: 10.3390/ma17235997
13. Han Y., Zou D., Kang Y., Zhong Z., Xing W. (2024): One-step sintering process for high-performance SiC membranes for efficient filtration of dust-laden gas. *Journal of Membrane Science, 692,* 122265. doi: 10.1016/j.memsci.2023.122265
14. Yu L., Zhang Y., Mao H., Cui K., Liu H. (2023): Structure evolution, properties and synthesis mechanism of ultra-lightweight eco-friendly ceramics prepared from kaolin clay and sewage sludge. *Journal of Environmental Chemical Engineering, 11*(1), 109061. doi: 10.1016/j.jece.2022.109061
15. Li C., Zhang P., Li D. (2022): Study on low-cost preparation of glass–ceramic from municipal solid waste incineration (MSWI) fly ash and lead–zinc tailings. *Construction and Building Materials, 356,* 129231. doi: 10.1016/j.conbuildmat.2022.129231

16. Jia C., Xu Z., Luo D., Xiang H., Zhu M. (2022): Flexible ceramic fibers: recent development in preparation and application. *Advanced Fiber Materials, 4*(4), 573-603. doi: 10.1007/s42765-022-00133-y
17. Fan J., Xu X., Niu S., Zhou Y., Li X., Guo Y., Luo Y. (2022): Anisotropy management on microstructure and mechanical property in 3D printing of silica-based ceramic cores. *Journal of the European Ceramic Society, 42*(10), 4388-4395. doi: 10.1016/j.jeurceramsoc.2022.03.059
18. Wei S., Han G., Zhang X., Sun J., et alJ. (2024): Preparation of high performance dense Al_2O_3 ceramics by digital light processing 3D printing technology. *Ceramics International, 50*(1), 2083-2095. doi: 10.1016/j.ceramint.2023.10.316
19. Chen Z., Yan W., Li G., Hong S., Li N. (2024): Enhanced mechanical properties of novel Al_2O_3-based ceramic filter by using microporous corundum-spinel and nano-Al_2O_3 powders. *Journal of the European Ceramic Society, 44(*2), 1070-1080. doi: 10.1016/j.jeurceramsoc.2023.10.004
20. Guo X., Wang H., Tian R., Yin H., Qiu Y., Wang F. (2022): Optimization of preparation process and characterization for hydrophobic α-Al_2O_3 ceramic membrane. *Materials Chemistry and Physics, 276*, 125280. doi: 10.1016/j.matchemphys.2021.125280
21. Li D., He C., Wang Y. S., Su W., Zhang F., Xu H. (2023): High purity Al2O3 ceramic: Metallizing strategy, microstructure and sealing properties. *Journal of Asian Ceramic Societies, 11*(2), 250-259. doi: 10.1080/21870764.2023.2195288
22. Yin Z., Liang G., Bi J. (2023): High strength and hardness BNNSs/Al_2O_3 composite ceramics prepared by hot-press sintering of in-situ composite BNNSs/Al_2O_3 powder. *Ceramics International, 49*(19), 31794-31801. doi: 10.1016/j.ceramint.2023.07.134
23. Shumilov V., Kirilin A., Tokarev A., Boden S., et al. (2022): Preparation of γ-Al_2O_3/α-Al_2O_3 ceramic foams as catalyst carriers via the replica technique. *Catalysis Today, 383,* 64-73. doi: 10.1016/j.cattod.2020.09.019
24. Malinverni C., Salvo M., De Zanet A., D'Isanto F., et al. (2023): Glass-ceramics for joining oxide-based ceramic matrix composites (Al_2O_3f/Al_2O_3-ZrO_2) operating under direct flame exposure. *Journal of the European Ceramic Society, 43*(8), 3621-3629. doi: 10.1016/j.jeurceramsoc.2023.02.019
25. Vemoori R., Bejugama S., Khanra,A. K. (2023): Fabrication and characterization of alumina and zirconia-toughened alumina porous structures. *Ceramics International, 49*(13), 21708-21715. doi: 10.1016/j.ceramint.2023.03.310
26. Alsubei M. D., Reid B., Aljlil S. A., Coppens M. O., Campos L. C. (2024): Fabrication and characterization of coated ceramic membranes from natural sources for water treatment applications. *Journal of Membrane Science, 690,* 122226. doi: 10.1016/j.memsci.2023.122226
27. Besisa N. H., Besisa D. H., Ewais E. M. (2022): Processing of high temperature alumina/aluminum titanate ceramic composites from clean sources. *Scientific Reports, 12*(1), 5957. doi: 10.1038/s41598-022-09670-3
28. Sekaran P. R., Ramakrishnan H., Venkatesh R., Nithya A. (2023): Mechanical and physical characterization studies of nano ceramic reinforced Al–Mg hybrid nanocomposites. *Silicon, 15*(10), 4555-4567. doi: 10.1007/s12633-023-02473-9
29. Alves C. L., Skorych V., De Noni Jr A., Hotza D., González S. G., Heinrich S. (2024): Optimizing raw material composition to increase sustainability in porcelain tile production: A simulation-based approach. Journal of the American Ceramic Society, 107(4), 2110-2127. doi: 10.1111/jace.19581

[30] Usman J., Salami B. A., Gbadamosi A., Adamu H., et al. (2023): Intelligent optimization for modelling superhydrophobic ceramic membrane oil flux and oil-water separation efficiency: Evidence from wastewater treatment and experimental laboratory. Chemosphere, 331, 138726. doi: 10.1016/j.chemosphere.2023.138726